Available online at www.sciencedirect.com

SciVerse ScienceDirect

Ceramics International 38 (2012) 3841–3849

CERAMICS INTERNATIONAL

www.elsevier.com/locate/ceramint

Enhanced ferroelectric properties of La-substituted $BiFeO_3$ thin films on $LaSrCoO_3/Pt/TiO_2/SiO_2/Si$ (1 0 0) substrates prepared by the soft chemical method

A.Z. Simões [a,*], M.A.Ramirez [a,1], C.R. Foschini [c,3], F. Moura [b,2], J.A. Varela [c,3], E. Longo [c,3]

[a] Universidade Estadual Paulista – Unesp – Faculdade de Engenharia de Guaratinguetá, Av. Dr. Ariberto Pereira da Cunha, 333, Bairro Pedregulho, CEP 12516-410, Guaratinguetá, SP, Brazil

[b] Universidade Federal de Itajubá – Unifei – Campus Itabira, Rua São Paulo, 377, Bairro: Amazonas, CEP 35900-37, Itabira, MG, Brazil

[c] Universidade Estadual Paulista – Unesp – Instituto de Química, Rua Professor Francisco Degni 55, Bairro Quitandinha, CEP 14800-900, Araraquara, SP, Brazil

Received 17 November 2011; received in revised form 12 January 2012; accepted 13 January 2012
Available online 21 January 2012

Abstract

$Bi_{0.85}La_{0.15}FeO_3$ (BLFO015) thin films were deposited by the polymeric precursor solution on $La_{0.5}Sr_{0.5}CoO_3$ substrates. For comparison, the films were also deposited on Pt bottom electrode. X-ray diffraction data confirmed the substitutions of La into the Bi site with the elimination of all secondary phases under a substitution ratio $x = 15\%$ at a temperature of 500 °C for 2 h. A substantial increase in the remnant polarization (P_r) with $La_{0.5}Sr_{0.5}CoO_3$ bottom electrode ($P_r \approx 34\ \mu C/cm^2$) after a drive voltage of 9 V was observed when compared with the same film deposited on Pt substrate. The leakage current behavior at room temperature decreased from 10^{-8} (Pt) to 10^{-10} A/cm^2 on ($La_{0.5}Sr_{0.5}CoO_3$) electrode under a voltage of 5 V. The fatigue resistance of the Au/BLFO015/LSCO/Pt/TiO_2/SiO_2/Si (1 0 0) capacitors with a thickness of 280 nm exhibited no degradation after 1×10^8 switching cycles at a frequency of 1 MHz.

Keywords: A. Films; B. Interfaces; C. Dielectric properties; C. Ferroelectric properties

1. Introduction

Revival in multiferroic materials brings ever-increasing enthusiasm in the research of this field [1]. Several promising materials such as YMnO3 [2], $LuFe_2O_4$ [3], $BiFeO_3$ (BFO) [4], and $BiMnO_3$ [5], are currently under intensive studies. Among them, BFO receives most of the interest due to its room temperature ferroelectric and magnetic orders [6,7]. In the traditional chemical method for preparing BFO based films, generally Pt/Ti/SiO_2/Si has been used as substrate; however, the poor ferroelectric–electrode interface prevents the full expression of the outstanding ferroelectric behavior of BFO thin films [8].

$BiFeO_3$ (BFO) crystallizes in a rhombohedrally distorted perovskite structure with both ferroelectric ($T_c \approx 830$ °C) and antiferromagnetic ($T_N \approx 370$ °C) characteristics [9,10]. The specific characteristics, such as simple crystal structure, high Curie temperature (electrical), and high Néel temperature (magnetic), are advantageous for research and various applications. However, it is well known that BFO suffers from high leakage currents, which in turn lead to an unsaturated *P–E* hysteresis loop at room temperature if care are not taken on the control of the processing parameters such as the oxygen partial pressure during the pulsed laser deposition process and the annealing temperatures [11,12]. The leakage current problem is more severe for BFO films prepared on Pt/Ti/SiO_2/Si substrates using the chemical solution deposition methods. Although the leakage current of BFO films can be reduced by doping with high valence ions such as Ti^{4+} and Nb^{5+}, saturated ferroelectric hysteresis loops are not observed in $BiFe_{1-x}Ti_xO_3$ and $BiFe_{1-x}Nb_xO_3$ films [13,14]. Recently, Singh et al. [15] have reported that the leakage current density of BFO films can be

* Corresponding author. Tel.: +55 12 3123 2228.
E-mail address: alezipo@yahoo.com (A.Z. Simões).
[1] Tel.: +55 12 3123 2228.
[2] Tel.: +55 31 3834 6472/6136.
[3] Tel.: +55 16 33019828.

0272-8842/$36.00
doi:10.1016/j.ceramint.2012.01.034

decreased by doping with Mn^{3+} ions at Fe^{3+} sites. The enhancement of the ferroelectric properties can also be found in Cr-doped $BiFeO_3$ films [16]. This suggests that isovalent ion substitution is more effective not only in reducing the leakage current but also in improving the ferroelectric properties of BFO films compared to the substitution using high valence ions.

Conductive oxides wit perovskite structure are expected to have much better affinity with a ferroelectric oxide which is more advantage for the interfacial properties between the conductive and ferroelectric oxides because of their similar crystal structures. So far, conductive oxides, such as $SrRuO_3$, $La_{0.5}Ca_{0.5}CoO_3$, $LaNiO_3$ (LNO), and $BaPbO_3$ [17–19], have been investigated and employed as electrodes to minimize the fatigue and aging of ferroelectric films, which is of the fundamental importance for the practical applications in multifunctional devices. Among these oxide electrode materials, $LaSrCoO_3$ (LSCO), which is a perovskite related metallic oxide [20], has also attracted much attention in recent years, as a conduction layer for application in ferroelectric memories. Because LSCO has a structure similar to that of perovskite ferroelectrics, textured and epitaxially grown LSCO film is a promising oxide electrode. At present, most epitaxial LSCO films have been prepared by physical processes such as pulsed laser deposition (PLD) [21] and RF magnetron sputtering [22]. A chemical solution process provides a simple and versatile alternative for crystalline thin film preparation [23,24]. LSCO has low resistivity and pseudo-cubic perovskite structure with lattice parameter 0.3835 nm, which is compatible with that of BFO (i.e., 0.396 nm). It is easy to fabricate LSCO on Pt coated Si substrate via a chemical route, and moreover, LSCO is inclined to grow in (1 1 1)-preferential orientation; thus, it is likely to induce the growth of BFO films in (1 1 1) orientation. All of these make it a good choice as buffer layer and bottom electrode. In this study we report the growth of effect of La-substituted BFO films deposited on LSCO/Pt/TiO_2/SiO_2/Si (1 0 0)Si substrates by using the polymeric precursor method and compare its structure and electrical properties with the growth of these films on traditional Pt/TiO_2/SiO_2/Si (1 0 0)Si substrates.

2. Experimental details

The LSCO bottom electrode thin film were spin coated (KW-4B, Chemat Technology) on (1 0 0) Pt/Ti/SiO_2/Si substrates by a commercial spinner operating at 5000 revolutions/min for 30 s. Each annealing layer was pre-fired at 400 °C for 2 h in a conventional oven. After the pre-firing, each layer was crystallized in a conventional furnace under an oxygen flow of 50 cm^3/min at 800 °C for 1 h employing six layers. Using the same procedure, the $Bi_{0.85}La_{0.15}FeO_3$ (BLFO015) thin films were deposited by spinning the precursor solution on the desired substrates at 500 °C for 2 h employing 10 layers. Through this process, we have obtained thickness values of about 150 nm for the bottom electrodes and around 280 nm for BLFO015. Phase analysis of the films were performed at room temperature by X-ray diffraction (XRD) patterns recorded on a (Rigaku-DMax 2000PC) with Cu-Kα radiation in the 2θ range from 20° to 60° with 0.3°/min.

The annealed thin film thickness was determined using scanning electron microscopy (SEM) (Topcom SM-300) by checking the cross-section where back-scattered electrons were utilized. Three measurements were taken to obtain an average thickness value. Microstructural characterization of the films was carried out using transmission electron microscopy (TEM) with a 200 kV Model CM200 Philips, Holland. The films were cutted in small pieces and a sandwich with thickness of 0.3 mm was acquired after polish. TEM samples were deposited on a carbon-covered Cu grid for analyses. Raman measurements were taken using an ISA T 64000 triple monochromator. An optical microscope with a 80× objective was used to focus the 514.5-nm radiation from a Coherent Innova 99 Ar^+ laser on the sample. The same microscope was used to collect the back-scattered radiation. The scattering light dispersed was detected by a charge-coupled device (CCD) detection system. A PHI-5702 multifunction X-ray photoelectron spectrometer (XPS) was used, with an Al-Kα X-ray source of 29.35 eV passing energy. The chamber pressure during the experiments was about 4.5×10^{-9} Torr. The calibration of the binding energy scale was controlled using the O1's line which appears in photoelectron spectra of the as-grown samples. The surface morphology of BLFO015 thin films was measured by atomic force microscopy (AFM) using a tapping mode technique (Nanoscope IIIa-Bruker). Then, a 0.5 mm diameter top Au electrode was sputtered through a shadow mask at room temperature. After deposition of the top electrode, the film was subjected to a post-annealing treatment in a tube furnace under an oxygen atmosphere at 300 °C for 1 h. Here, the desired effect was to eventually decrease present oxygen vacancies. The electric properties were measured by an Au/BLFO015/LSCO/Pt/Ti/SiO_2/Si (1 0 0) and Au/BLFO015/Pt/Ti/SiO_2/Si (1 0 0) capacitor structures. The hysteresis loop measurements were carried out on the films with a Radiant Technology RT6000HVS at a measured frequency of 60 Hz. These loops were traced using the Charge 5.0 program included in the software of the RT6000HVS in a virtual ground mode test device. The capacitance–voltage characteristic was measured using a small AC signal of 10 mV at 100 kHz. The AC signal was applied across the sample, while the DC was swept from positive to negative bias. The *J–V* measurements were recorded on the Radiant Technology tester in the current–voltage mode, with a voltage changing from 0 to +10 V, from +10 to −10 V and back to 0 V. For the fatigue measurements, internally generated 8.6 μs wide square pulses or externally generated square pulses were used with a 10 mV amplitude. All measurements were taken at room temperature.

3. Results and discussions

3.1. X-ray diffraction analyses

Fig. 1 shows the XRD pattern of the BLFO015 film on LSCO/Pt/Ti/SiO_2/Si (1 0 0) and BLFO015/Pt/Ti/SiO_2/Si (1 0 0) substrates. The pattern of the BFO film was indexed

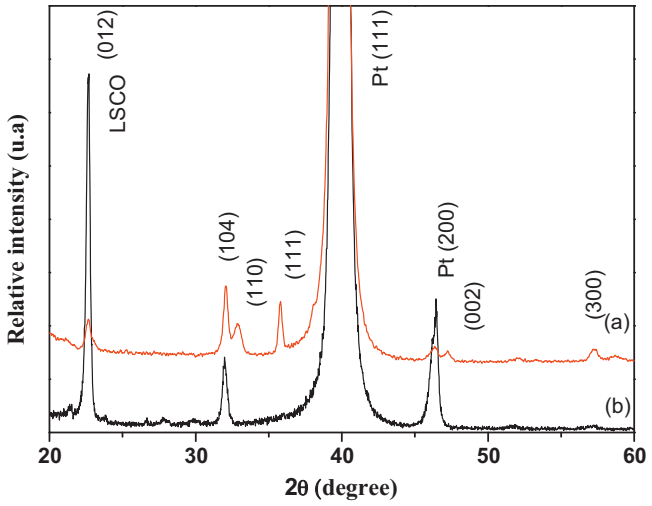

Fig. 1. X-ray diffraction of a $Bi_{0.85}La_{0.15}FeO_3$ thin film deposited by the polymeric precursor method and annealed at 500 °C in static air for 2 h on: (a) LSCO and (b) Pt.

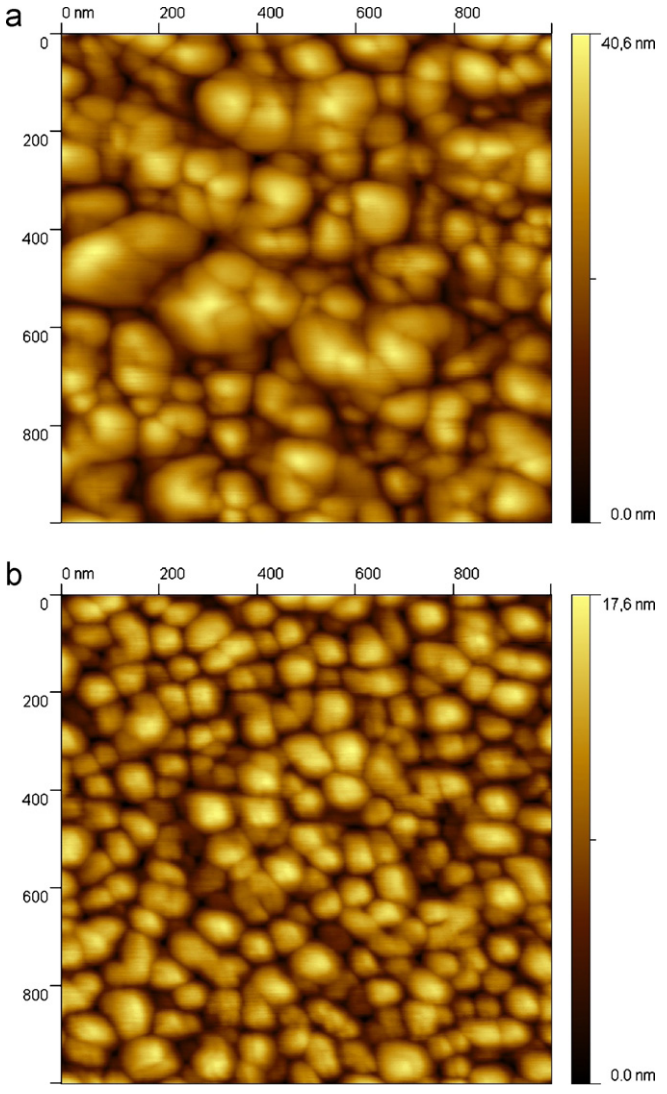

Fig. 2. AFM micrograph of a $Bi_{0.85}La_{0.15}FeO_3$ thin film deposited by the polymeric precursor method and annealed at 500 °C in static air for 2 h on: (a) LSCO and (b) Pt.

according to ICSD 72-2035. From Fig. 1 we can see that the film is fully crystallized since extremely intense and thin peaks are evident and no impure phase such as $Bi_2Fe_4O_9$ and $Bi_{46}Fe_2O_{72}$ phases are observed. According to the pattern, the film has a rhombohedral perovskite structure. Furthermore, it is randomly oriented. As shown in Fig. 1, the strongest peak of the LSCO thin film corresponds to non-oriented LSCO (1 1 0) grains with perovskite structure being its position in the pattern coincident with the BLFO015 (0 1 2) orientation. It was found that all the films consisted of a single phase showing preferred (0 1 2) and (1 1 1) orientations. The XRD results clearly show that films deposited on LSCO electrode favors the growth of (1 1 1)-oriented grains whereas in films deposited on Pt the growth of (0 1 2) oriented grains dominated. Some orientation-sensitive physical properties, such as dielectric permittivity, remanent polarization and drive voltage, should vary with the extent of mixed orientations which are different for the films grown on different electrodes. However, this behavior was not observed for films with lanthanum content superior than 15.0% (not shown in the article). According to Zhang et al. [25], for lanthanum contents higher than 15.0% the rhombohedral structure decreases. This structural distortion might be responsible for the high leakage and lower remnant polarization of the $Bi_{0.7}La_{0.30}FeO_3$ system. The here discussed preferred orientations can be caused by differences in lattice parameters and thermal expansion coefficients for different oxide electrodes and indicate that the polar axis is closer to (1 1 1) than (0 1 2).

3.2. AFM and TEM analyses

To confirm the surface morphology, AFM was carried out. The results are shown in Fig. 2. Changes on the surface morphology of the BLFO015 films were evaluated. AFM studies revealed that independently of the bottom electrode homogeneous surface was observed indicating that the polymeric precursor method allows the preparation of films with controlled morphology. The average surface roughness value is 4.3 nm for the film deposited on Pt electrode and 7.5 nm for the film deposited on LSCO bottom electrode. The average grain size is 58 and 85 nm, respectively. It was also found that the Pt electrode tends to suppress the grain growth. These results are consistent with the XRD results where a decrease in peak sharpness and intensity was observed with Pt electrode. La-substitution was found to be effective in improving the surface morphology of synthesized BFO-based films, because the precursor film underwent the optimized nucleation and growth process producing films with a homogeneous and dense microstructure. Also, the homogeneous microstructure of BLFO015 films may affect the ferroelectric properties, because the voltage can be applied uniformly onto it.

In order to evaluate the role exerted by the bottom electrode on the microstructure of BLFO015 film, we present TEM

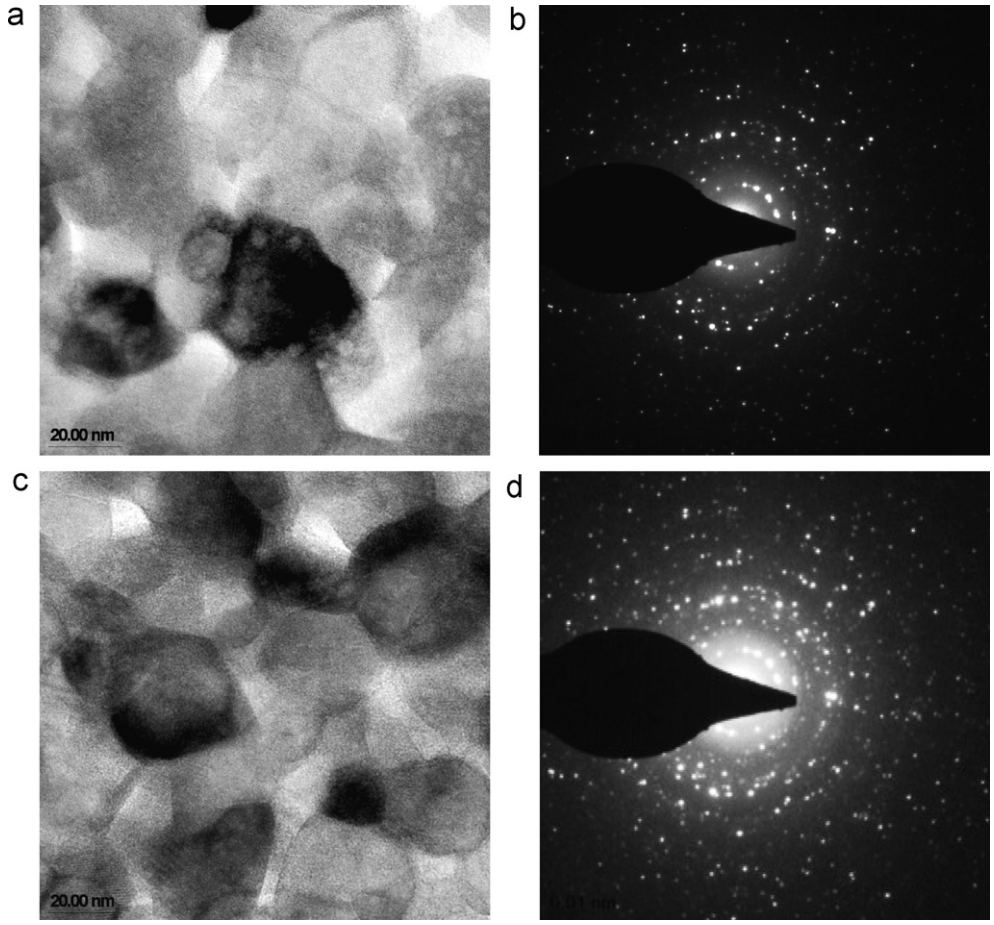

Fig. 3. TEM and SAD micrographs of a $Bi_{0.85}La_{0.15}FeO_3$ thin film deposited by the polymeric precursor method and annealed at 500 °C in static air for 2 h on: (a) and (b) LSCO bottom electrode and (c) and (d) Pt bottom electrode.

images of both samples. A plan-view TEM image shows the microstructure and the selected area diffraction (SAD) patterns. It could be noticed the polycrystallinity of the grains in the plane of the films. The grains are regularly shaped and the estimates size obtained from dark field images is about 80 nm for BLFO015 film deposited on LSCO bottom electrode and 60 nm for BLFO015 film deposited on Pt electrode (Fig. 3a and c, respectively). Tiny pores less than 10 nm in size are present within the grains and along the grain boundaries. The role of oxide bottom electrode is to eliminate vacancies which act as point defects and therefore decrease the surface heterogeneity in the films. The decrease of grain size of BLFO015 films deposited on Pt electrode can be interpreted by slower oxygen ion motion and consequently lower grain growth rate. In this way, the lower grain size can be a reflex of increase in crystallization temperature due to differences of chemical bond strength between Fe–O, La–O and Pt atoms. From TEM analyses we could observe that the cristallinity of materials is good and the presence of non crystalline phase is not evident. Besides that, the diffraction patterns indicate strong randomness of atom position in Pt electrode, as previous noted in the XRD data (Fig. 3b) and weak randomness of atom position in LSCO electrode. In this way, we assume that the bottom electrode has strong effect on crystal structure of BLFO015 films (Fig. 3d) and as could be seen, the electrical properties of those films will shown remarkable difference.

3.3. XPS and micro-Raman analyses

To identify the chemical bonding of BLFO015 thin films XPS studies were performed. The spectrum expanded from 700 eV to 745 eV (see Fig. 4). The 3/2 and 1/2 spin–orbit doublet components of the Fe 2*p* photoemission located at 711.1 and 724.6 eV, respectively were identified as Fe^{3+}; there is no evidence of Fe^{2+} and Fe in the XPS spectra. XPS results show that BLFO015 thin films on both bottom electrodes have a single phase with a Fe^{3+} valence state which is consistent with XRD results shown in Fig. 1. The oxidation state of Fe was purely 3+, which was advantageous for producing BLFO015 film with low leakage current.

Raman spectra of BLFO015 thin films deposited on both electrodes show the order-disorder degree of the atomic structure at short range (Fig. 5). The modes further split into longitudinal and transverse components due the long electrostatic forces associated with lattice ionicity. Lanthanum atoms substitute bismuth within the perovskite structure having marginal influence in the interactions between the $(Bi_2O_2)^{2+}$ layers and perovskite. The vibrational modes located at 224,

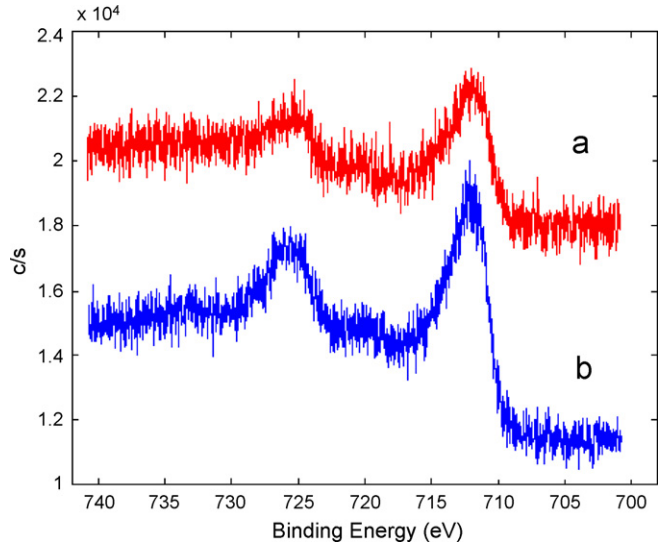

Fig. 4. XPS analysis of a $Bi_{0.85}La_{0.15}FeO_3$ thin film deposited by the polymeric precursor method and annealed at 500 °C in static air for 2 h (Fe 2*p* peaks) on: (a) LSCO and (b) Pt.

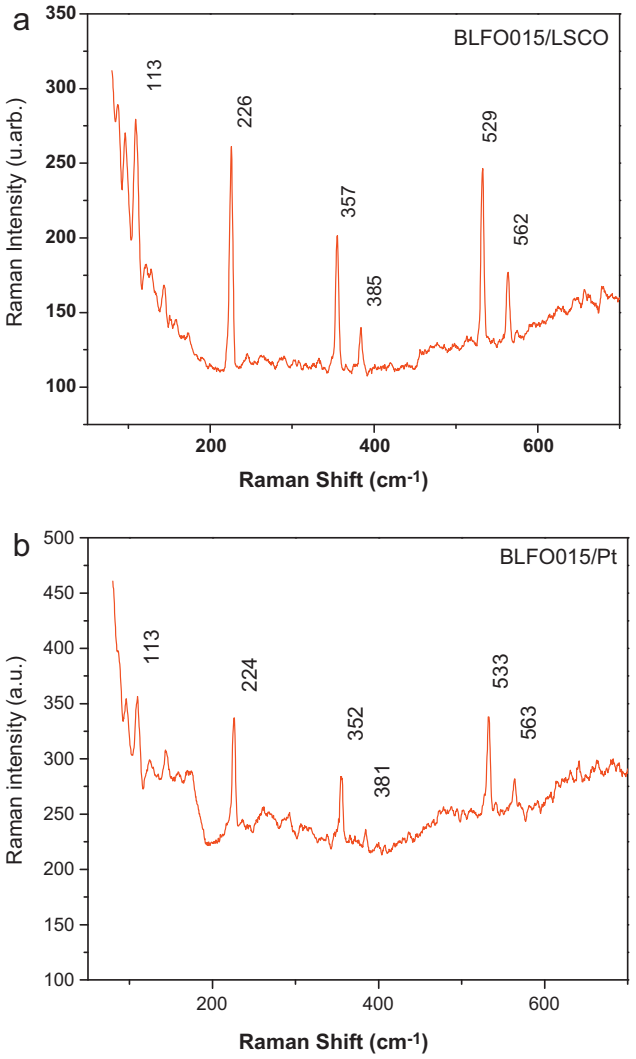

Fig. 5. Micro-Raman spectra for $Bi_{0.85}La_{0.15}FeO_3$ film deposited by the polymeric precursor method and annealed at 500 °C in static air for 2 h on: (a) LSCO and (b) Pt.

355, 385, 531, and 564 cm^{-1} result from the FeO_6 octahedral (Fe = 5 or Fe = 6). The band located below 200 cm^{-1} is due to the different sites occupied by bismuth within the perovskite layer. Slight changes which occur above 200 cm^{-1} in the BLFO015 can be associated to structural distortion and reduction of vibrations in the FeO_5 octahedra. The vibrational modes of the film deposited on Pt electrode tend to disappear when compared to the film deposited on LSCO bottom electrode. During the energy transfer process specific structural rearrangements take place and a remarkable solution of the distortion across the octahedral (FeO_6) and dodecahedral (BiO_{12}) clusters can be evidenced. In this way, there is a symmetry breaking process along the network of both [FeO_6] and [BiO_{12}] clusters leading to lower symmetry. This can be related to structural disordering at short range, as well as a phase transition for an ordering crystal structure. The structural changes developed at the Pt interface create localized levels in the band gap and an inhomogeneous charge distribution between valence and conduction bands.

3.4. Dielectric properties analyses

Fig. 6 illustrates the *C–V* curve for BLFO015 films obtained at 100 kHz and DC sweep voltage from +10 to −10 V. The capacitance–voltage dependence is strongly nonlinear, confirming the ferroelectric properties of the film resulting from domain switching. BLFO015 films deposited on LSCO bottom electrode present a symmetric *C–V* curve around the zero bias axis, indicating that the films contain only few movable ions or charge accumulation at the film–electrode interface. Although the *P–E* hysteresis is saturated at ≥5 V the *C–V* curve shows hysteresis up to ±10 V because both measurements were performed at different frequencies where the domain alignment is a time dependent process and plays an important role in the switching behavior of the domains. Therefore, the sweep voltage ranges differ greatly (5 V) and consequently also the (*dV*/*dt*) voltage sweep per time unit leading to different domain alignment kinetics. The narrowing of the *C–V* curve obtained for the film deposited on LSCO bottom electrode indicates that the switching process of domains is faster and the saturation occurs with low energy for the ferroelectric domain alignment. On the other hand, for films deposited on Pt a slight change in capacitance values is observed indicating that exist charge carriers (oxygen vacancies) trapped near the film–electrode interface. These charges may be originated during the heat treatment process due to the decomposition of the polymeric precursor [26]. It can be assumed that if oxygen vacancy accumulation near the film–electrode interface occurs during heat treatment, the LSCO conductive oxide can consume the oxygen vacancies by changing their oxygen nonstoichiometry and thus, the accumulation of oxygen vacancies near the interface is prevented or reduced.

Fig. 7 shows the leakage currents density as a function of voltage measured at room temperature. The curve was recorded

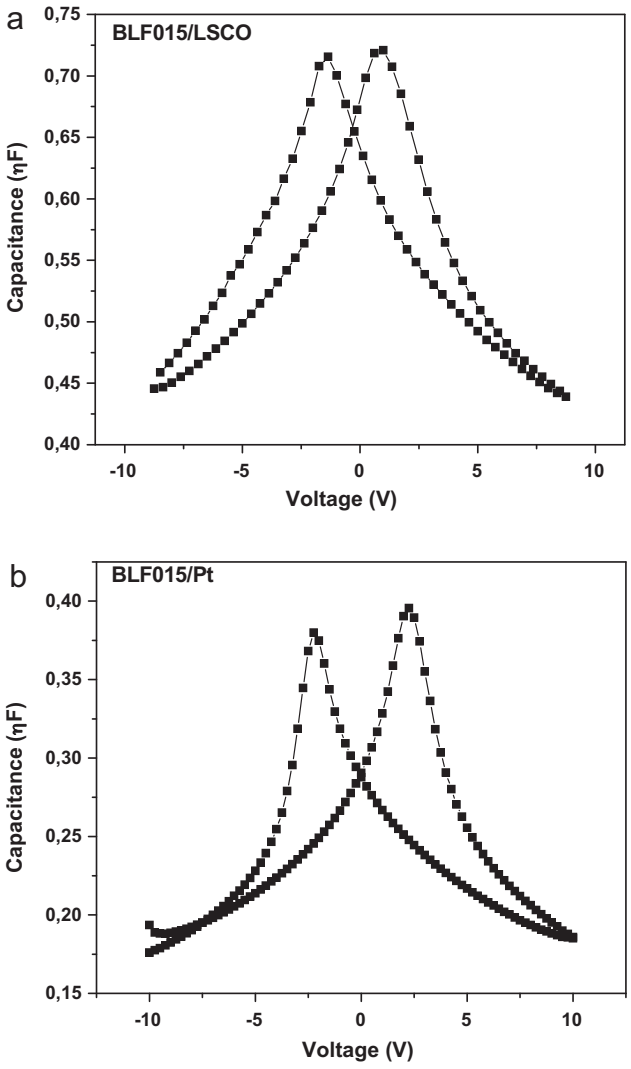

Fig. 6. Capacitance–voltage dependence for $Bi_{0.85}La_{0.15}FeO_3$ film deposited by the polymeric precursor method and annealed at 500 °C in static air for 2 h on: (a) LSCO and (b) Pt.

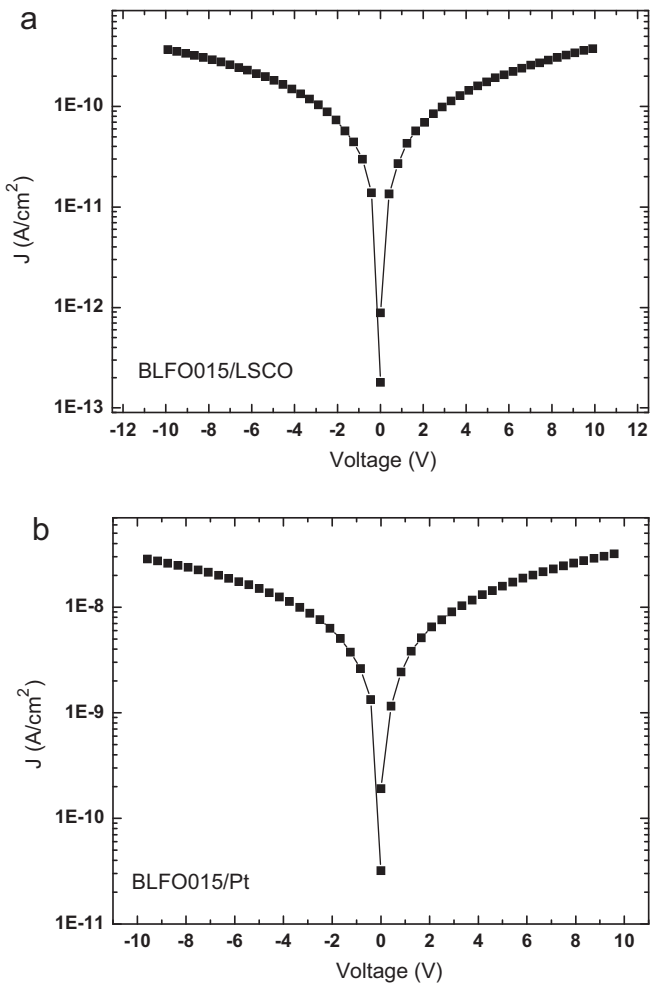

Fig. 7. Leakage current density versus applied voltage for a $Bi_{0.85}La_{0.15}FeO_3$ thin film deposited by the soft chemical method and annealed at 500 °C in static air for 2 h on: (a) LSCO and (b) Pt.

with a voltage step width of 0.1 V and elapsed time of 1.0 s for each voltage. The measured logarithmic current density (log J) versus the voltage (V) is symmetric and shows two clearly different regions. The insulating properties of the films were found to be dependent on the bottom electrode. The leakage current density decreased for the films deposited on LSCO bottom electrode. Such a reduction in leakage current density may be attributed to high oxygen affinity of the LSCO bottom electrode avoiding that oxygen in the electrode material will be depleted by the ferroelectric material, thus leaving an oxygen deficient layer of the electrode at the interface and increasing the contact resistance. From this study it can be demonstrated that the microstructures of ferroelectric films play an important role in their conductivity properties [27]. Comparing with literature data, our films present a lower leakage current than the films obtained on highly oriented $LaNiO_3$-buffered Pt/Ti/SiO_2/Si substrates by a RF magnetron sputtering [28]. Since the conductivity is strongly affected by the characteristics of the film–electrode interface, the lower leakage current observed in our case may be attributed probably to differences in grain size, density, and preferred orientation due to differences in the ferroelectric material and the interface. The current density increases linearly with the external voltage in the region of low applied voltage strengths which suggests an ohmic conduction. At higher field strengths, the current density increases exponentially which implies that at least one part of the conductivity results from the Schottky or Poole-Frenkel emission mechanism. The leakage current density at 5.0 V changes from 10^{-10} (LSCO) to 10^{-8} A/cm^2 (Pt). The main reason for such a small value can be attributed to changes in the surface roughness and the reduction of microcracks due to modification on the interface stability on oxide electrode. Thus, LSCO bottom electrode reduces oxygen vacancies improving switching process of ferroelectric domains.

3.5. Ferroelectric properties analyses

The room temperature P–E hysteresis loop of BLFO015 thin films deposited on LSCO and Pt electrodes are shown in Fig. 8a and b. The loop deposited on LSCO bottom electrode is well

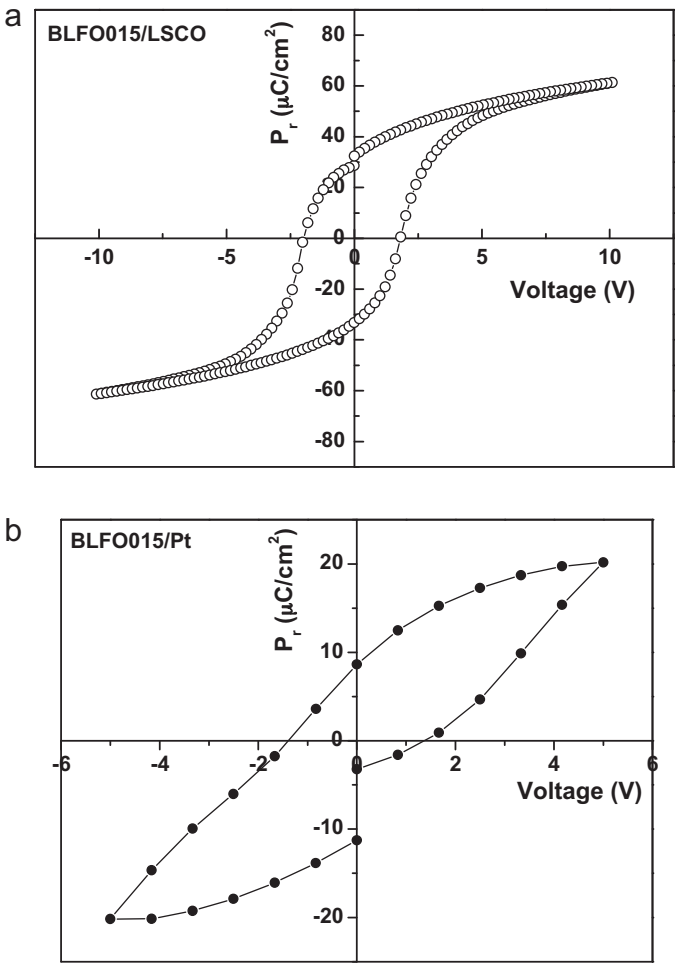

Fig. 8. Hysteresis loop of a $Bi_{0.85}La_{0.15}FeO_3$ thin film deposited by the polymeric precursor method and annealed at 500 °C in static air for 2 h on: (a) LSCO and (b) Pt.

saturated and rectangular with a $P_r \sim 34$ μC/cm^2 after applying a voltage of 10 V. No sign of leakage has been observed under a measuring frequency of 60 Hz. Liu et al. [29] have reported substantially reduced leakage of $BiFeO_3$ films by introducing a $LaNiO_3$ intermediate layer. Although a saturated hysteresis loop was observed, they obtained only a remanent polarization of 26.9 μC/cm^2 under 1.25 MV/cm. To our knowledge, there have been very few reports on a large P_r and a rectangular loop of BLFO015 film obtained from chemical methods [30,31]. Meanwhile, the hysteresis loop in our work is more saturated than some of the BFO film on the Pt bottom electrode by the chemical solution deposition method [32]. In fact, the pure BFO film loops on the Pt bottom electrode are unsaturated in some cases. Gonzalez et al. [33] observed saturated hysteresis loops at room temperature in pure BFO films on a Pt bottom electrode while they observed a remnant polarization ~ 36 μC/cm^2 under 800 kV/cm. In other typical studies from Singh et al. [34], Hu et al. [35] and Uchida et al. [36] unsaturated loops were observed under 10 kHz at room temperature for BFO films deposited under Pt bottom electrode. Our results are comparable to those observed in the epitaxial BFO films on a (1 0 0) $SrTiO_3$ substrate prepared by the PLD method [37]. The film presents well-saturated hysteresis characteristics with a remanent polarization (P_r) of 31 μC/cm^2 and a coercive field (E_c) of 560 kV/cm at a maximum applied electric field of 1000 kV/cm. According to Wang et al. [4] the BFO ferroelectricity originates from the relative displacements of a Bi ion and a Fe–O octahedron along the (1 1 1) orientation in epitaxial BFO thin films and the projection polarization along the (1 1 0) orientation is larger than the polarization of the (1 0 0) orientation. Since our films are intense (1 1 1) we reasonably expect a larger polarization on LSCO bottom electrode. A moderate coercive field probably originates from the intermediary grain size (85 nm) of the BLFO015 thin films deposited on LSCO electrode. However, for the film deposited on Pt electrode the trapped charge (O_2') associated with other defects ($V_0^{\bullet\bullet}$) or even defect dipole complexes such as oxygen vacancies associated to bismuth vacancies ($V'''_{Bi} - V_0^{\bullet\bullet}$) located in the grain boundary and in the film–electrode interface can promote a local stoichiometry deviation influencing the shape of the hysteresis loops. As a consequence of these space charges, a significant shift along the electric field axis towards the positive bias, which is defined as imprint, may lead to a failure of the capacitor. A more symmetric hysteresis loop is observed for the film deposited on LSCO electrode indicating that the high oxygen affinity of this material avoids the migration of charge species to the electrode–film interface. This behavior can be ascribed to the larger grains of the BLFO015 thin films deposited on LSCO bottom electrode. The domain walls in larger grains are easier to be switched under external field. Similar phenomena have been found in $SrBi_2Ta_2O_9$ and $PbTiO_3$ thin films [38,39]. The polarization switching in films with small grains is usually more difficult, as in the case of Pt electrode. Therefore, the growth of the film in one direction not coincident to *c*-axis preferred orientation will favor larger grains morphology, such as the ones grown on LSCO bottom electrode leading to a lower E_c when compared to those grown on Pt. The BLFO015 thin film deposited on Pt electrode exhibits a poor *P–E* hysteresis loop, which has been typically observed from conductive ferroelectrics and it get breakdown with increased bias electric field due to a large leakage current. The ferroelectric properties of BLFO015 thin film may be related to two main factors: one is the increased rattling space of the oxygen octahedron due to larger La atom, and the other is the decreased grain size with Pt electrode, since the strength of polarization is strongly related to the grain size [40]. It has been found that the polarizability in perovskites (ABO_3) is partially related with the sizes of A and B cations. In general, a large A cation results in an increase in polarizability, since the large A cation leads to "a larger rattling space" available for B cation by increasing the size of the oxygen octahedron. The increased remnant polarization of BLFO015 thin film on LSCO bottom electrode can be explained by the substitution of larger La (1.172 Å) ions for a part of Bi (1.03 Å) ions in BFO. In the case of the film deposited on Pt electrode, the decreased volume fraction of dielectric polarization with decreasing grain size could have predominant effect on the remnant polarization.

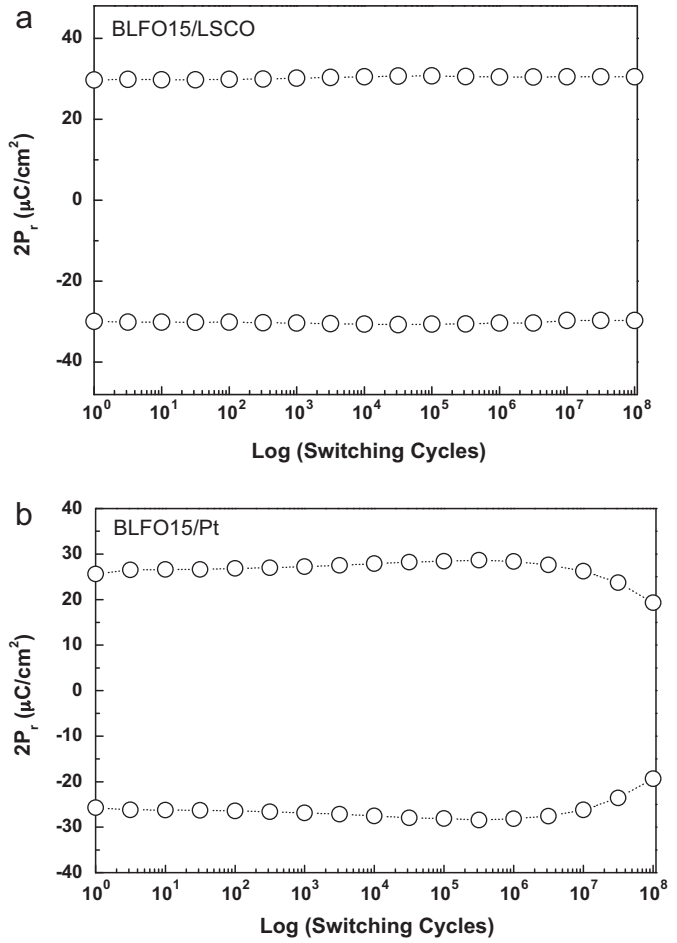

Fig. 9. Fatigue properties of a $Bi_{0.85}La_{0.15}FeO_3$ thin film deposited by the polymeric precursor method and annealed at 500 °C in static air for 2 h on: (a) LSCO and (b) Pt.

Fig. 9 plots the degradation of normalized switchable polarization $\Delta P = P^* - P^\wedge$ of the BLFO015-based films against the number of switching cycles. P^* represents the switching polarization between two pulses with opposite polarity, and $P^\wedge$ represents the nonswitching polarization between two pulses with the same polarity. Fatigue resistance was observed up to 10^8 cycles for the LSCO bottom electrode suggesting a good potential for applications in ferroelectric memories. Since LSCO bottom electrode result in fatigue-free films (Fig. 9a), it is consequently, to believe that if oxygen vacancy accumulation near the film–electrode interface occurs during fatigue, the conductive oxide can provide the oxygen to those vacancies by changing their oxygen nonstoichiometry and thus, the accumulation of oxygen vacancies near the interface is prevented or reduced. On the other hand, BLFO015-based films deposited on Pt electrode reveal an increase in local current around the nucleation sites which can damage the film–electrode interface and suppress the nucleation of oppositely oriented domains at the surface. In this film an increase in switching polarization leads to a local increase in conductivity at the film–electrode interface region [41]. The switchable polarization of the BLFO015-based films deposited on Pt shows 25.0% decay after 10^8 cycles. This film also showed good long-time retention characteristics, retaining 94% of the values measured at $t = 1 \times 10^4$ s for an applied electric field of 150 kV/cm. The polarization charge compensation by the redistribution of defect charges should be considered to explain this small retention loss in lanthanum doped bismuth ferrite thin films [42]. The LSCO bottom electrode can maintain the stability of the interface and bulk defects and solve the fatigue problem of BFO thin films. On the other hand, the film deposited on Pt can provide conductive electrons which reduce the polarization and increase the concentration of holes in the interface region. The marked improvement in the fatigue behavior of LSCO bottom electrode may result from the crystallinity, electrode/ferroelectric interface, and defect concentration. Further studies are required to understand the fatigue behavior of La-doped BFO films after at least 10^{12} switching cycles.

4. Conclusions

In summary, we have demonstrated a viable chemical deposition process which enables the growth of good quality La-based $BiFeO_3$ multiferroic thin films. The leakage-current density of the film deposited on LSCO was around 10^{-10} A/cm^2 with a remnant polarization P_r of 34 μC/cm^2 at room temperature. The low conductivity of the BLFO015 film on LSCO bottom electrode is a consequence of oxygen vacancies ordering which prevents oxygen ions from migrating and few conditions for the trapping of electrons as a consequence of a larger grain size of such film. A regularly shaped hysteresis loop is observed for the films deposited on the LSCO bottom electrode due to the high oxygen affinity which avoids the migration of charge species for the electrode–film interface. High fatigue resistance was observed for films deposited on LSCO bottom electrode indicating that this film could be used in non-volatile random access memories. However, due to the imprint phenomenon the film deposited on Pt electrode is unsuitable for memory applications as a consequence of the substantial difference between $+V_c$ and $-V_c$. A remarkable improvement in the remnant polarization and drive voltage suggest that BLFO015 thin films deposited on LSCO oxide electrode are suitable for integrated device applications and can be used for ferroelectric random access memories.

Acknowledgments

The financial support of this research project by the Brazilian research funding agencies CNPq and FAPESP is gratefully acknowledged.

References

[1] N.A Spaldin, M. Fiebig, The renaissance of magnetoelectric multiferroics, Science 309 (2005) 391–392.
[2] M. Fiebig, Th Lottermoser, D. Fröhlich, A.V. Goltsev, R.V. Pisarev, Observation of coupled magnetic and electric domains, Nature (London) 419 (2002) 818–820.
[3] N. Ikeda, H. Ohsumi, K. Ohwada, K. Ishii, T. Inami, K. Kakurai, Y. Murakami, K. Yoshii, S. Mori, Y. Horibe, H. Kito, Ferroelectricity from

iron valence ordering in the charge-frustrated system $LuFe_2O_4$, Nature (London) 436 (2005) 1136–1138.
[4] J. Wang, J.B. Neaton, H. Zheng, V. Nagarajan, S.B. Ogale, B. Liu, D. Viehland, V. Vaithyanathan, D.G. Schlom, U.V. Waghmare, N.A. Spaldin, K.M. Rabe, M. Wuttig, R. Ramesh, Epitaxial $BiFeO_3$ multiferroic thin film heterostructures, Science 299 (2003) 1719–1722.
[5] M. Gajek, M. Bibes, S. Fusil, K. Bouzehouane, J. Fontcuberta, A. Barthélémy, A. Fert, Tunnel junctions with multiferroic barriers, Nat. Mater. 6 (2007) 296–302.
[6] F. Kubel, H. Schmid, Structure of a ferroelectric and ferroelastic monodomain crystal of the perovskite $BiFeO_3$, Acta Crystallogr. B: Struct. Sci. 46 (1990) 698–702.
[7] S.V. Kiselev, R.P. Ozerov, G.S. Zhdanov, Sov. Phys. Dokl. 7 (1962) 742–744.
[8] Y.H. Lee, J.M. Wu, Y.L. Chueh, L.J. Chou, Low temperature growth and interface characterization of $BiFeO_3$ thin films with reduced leakage current, Appl. Phys. Lett. 87 (2005) 172901–172903.
[9] J. Wang, J.B. Neaton, H. Zheng, V. Nagarajan, S.B. Ogale, B. Liu, Epitaxial $BiFeO_3$ multiferroic thin film heterostructures, Science 299 (2003) 1719–1722.
[10] S.Y. Yang, F. Zavaliche, L. Mohaddes-Ardabili, V. Vaithyanathan, D.G. Schlom, Y.J. Lee, Influence of La doping in multiferroic properties of $BiFeO_3$ thin films, Appl. Phys. Lett. 87 (2005) 1–3.
[11] J. Dho, X. Qi, H. Kim, J.L. MacManus-Driscoll, M.G. Blamire, Large electric polarization and exchange bias in multiferroic $BiFeO_3$, Adv. Mater. 18 (2006) 1445–1448.
[12] A.Z. Simões, A.H.M. Gonzalez, L.S. Cavalcante, C.S. Riccardi, E. Longo, J.A. Varela, Ferroelectric characteristics of $BiFeO_3$ thin films prepared via a simple chemical solution deposition, J. Appl. Phys. 101 (2007) 1–4.
[13] X. Qi, J. Dho, R. Tomov, M.G. Blamire, J.L. MacManus-Driscoll, Greatly reduced leakage current and conduction mechanism in aliovalention-doped $BiFeO_3$, Appl. Phys. Lett. 86 (2005) 062903–062905.
[14] C.F Chung, J.P. Lin, J.M Wu, Influence of Mn and Nb dopants on electric properties of chemical-solution-deposited $BiFeO_3$ films, Appl. Phys. Lett. 88 (2006) 1–3.
[15] S.K Singh, H. Ishiwara, K. Maruyama, Room temperature ferroelectric properties of Mn-substituted $BiFeO_3$ thin films deposited on Pt electrodes using chemical solution deposition, Appl. Phys. Lett. 88 (2006) 1–3.
[16] J.K. Kim, S.S. Kim, W. Kim, A.S. Bhalla, R. Guo, Enhanced ferroelectric properties of Cr-doped $BiFeO_3$ thin films grown by chemical solution deposition, Appl. Phys. Lett. 88 (2006) 1–3.
[17] A.M. Dhote, S. Madhukar, W. Wei, T. Venkatesan, R. Ramesh, C.M. Cotell, Direct integration of ferroelectric La–Sr–Co–O/Pb–Nb–Zr–Ti–O/La–Sr–Co–O capacitors on silicon with conducting barrier layers, Appl. Phys. Lett. 68 (1996) 1350–1352.
[18] K.S. Hwang, Y.M. Lee, S.S. Min, B.A. Kang, Epitaxially grown LaSr-CoO_3 thin films on various substrates by the sol–gel method, J. Sol-Gel Sci. Technol. 18 (2000) 175–180.
[19] K. Hwang, T. Manabe, I. Yamaguchi, S. Mizuta, T. Kumagai, Preparation of epitaxial $Pb(Zr,Ti)O_3$ thin films on MgO(1 0 0) substrates by dipping-pyrolysis process, J. Ceram. Soc. Jpn. 105 (1997) 952–956.
[20] K.H. Wong, W. Wu, P.W. Chan, J.T. Cheung, Low temperature growth of epitaxial LSCO films on (1 0 0) STO by pulsed laser deposition, Thin Solid Films 312 (1998) 7–10.
[21] S. Nagaraj, R. Aggarwal, R. Ramesh, Role of substrate on the dielectric and piezoelectric behavior of epitaxial lead magnesium niobate-lead titanate relaxor thin films, Appl. Phys. Lett. 77 (2000) 438–440.
[22] M.S. Chen, T.B. Wu, J.M. Wu, Effect of reducing atmosphere on electrical properties of sol–gel-derived $Pb(Zr,Ti)O_3$ ferroelectric films on textured $LaNiO_3$ electrode, Jpn. J. Appl. Phys. 40 (2001) 6045–6048.
[23] Y.R. Luo, J.M. Wu, $BaPbO_3$ perovskite electrode for lead zirconate titanate ferroelectric thin films, Appl. Phys. Lett. 79 (2001) 3669–3671.
[24] K. Hwang, T. Manabe, T. Nagahama, I. Yamaguchi, T. Kumagai, S. Mizuta, Effect of substrate materials on the crystallinity and epitaxy of $Pb(Zr,Ti)O_3$ thin films, Thin Solid Films 347 (1999) 106–111.
[25] T.S Zhang, M.H. Lu, D. Wu, Y.F. Chen, N.B. Ming, Larger polarization and weak ferromagnetism in quenched $BiFeO_3$ ceramics with a distorted rhombohedra crystal structure, Appl. Phys. Lett. 87 (2005) 262907–262909.
[26] J.F. Scott, C.A. Araujo, B.M. Melnick, L.D. McMillan, R. Zuleeg, Quantitative measurement of space-charge effects in lead zirconate–titanate memories, J. Appl. Phys. 70 (1991) 382–388.
[27] J. Zhai, H. Chen, Ferroelectric properties of $Bi_{3.25}La_{0.75}Ti_3O_{12}$ thin films grown on the highly oriented $LaNiO_3$ buffered $Pt/Ti/SiO_2/Si$ substrates, Appl. Phys. Lett. 82 (2003) 442–444.
[28] Y.H. Lee, J.M. Wu, Y.L. Chueh, L.J. Chou, Low-temperature growth and interface characterization of $BiFeO_3$ thin films with reduced leakage current, Appl. Phys. Lett. 87 (2005) 172901–172903.
[29] H. Liu, Z. Liu, K. Yao, Improved electric properties in $BiFeO_3$ films by the doping of Ti, J. Sol-Gel Sci. Technol. 47 (2007) 123–128.
[30] X.J. Meng, J.G. Cheng, J.L. Sun, H.J. Ye, Low-temperature preparation of highly (1 1 1) oriented PZT thin films by a modified sol–gel technique, J. Cryst. Growth 208 (2000) 541–545.
[31] W. Zhu, M.S. Tse, W. Lu, PZT capacitor with Ir/IrO2/Ir electrode fabricated by RTA Process, Integr. Ferroelectr. 12 (1996) 167–175.
[32] J.K. Kim, S.S. Kim, J.W. Kim, Substitution effects on the ferroelectric properties of $BiFeO_3$ thin films prepared by chemical solution deposition, J. Appl. Phys. 101 (2007) 014108–014110.
[33] A.H.M. Gonzalez, A.Z. Simões, L.S Cavalcante, Soft chemical deposition of $BiFeO_3$ multiferroic thin films, Appl. Phys. Lett. 90 (2007) 052906–052908.
[34] S.K. Singh, H. Ishiwara, K. Maruyama, Room temperature ferroelectric properties of Mn-substituted $BiFeO_3$ thin films, Appl. Phys. Lett. 88 (2006) 262908–262910.
[35] G.D. Hu, X. Cheng, W.B. Wu, C.H. Yang, Low leakage current and enhanced ferroelectric properties of Ti and Zn codoped $BiFeO_3$ thin film, Appl. Phys. Lett. 92 (2008) 192905–232911.
[36] H. Uchida, R. Ueno, H. Funakubo, S. Koda, Crystal structure and ferroelectric properties of rare-earth substituted $BiFeO_3$ thin films, J. Appl. Phys. 100 (2006) 014106–014114.
[37] Y. Wang, C.W. Nan, Enhanced ferroelectricity in Ti-doped multiferroic $BiFeO_3$ thin films, Appl. Phys. Lett. 89 (2006) 052903–052905.
[38] T. Li, Y. Zhu, S.B. Desu, C.H. Peng, M. Nagata, Metalorganic chemical vapor deposition of ferroelectric $SrBi_2Ta_2O_9$ thin films, Appl. Phys. Lett. 68 (1996) 616–618.
[39] A.L. Kholkin, V.V. Shvartsman, Y.A. Emelyanov, R. Poyato, M.L. Calzada, L. Pardo, Stress-induced suppression of piezoelectric properties in $PbTiO_3$:La thin films via Scanning Force Microscopy, Appl. Phys. Lett. 82 (2003) 2127–2129.
[40] Y. Shimakawa, Y. Kubo, Y. Tauchi, H. Asano, T. Kamiyama, F. Izumi, Z. Hiroi, Crystal, Electronic structures of $Bi_{4-x}La_xTi_3O_{12}$ ferroelectric materials, Appl. Phys. Lett. 79 (2001) 2791–2793.
[41] B.H. Park, S.J. Hyun, S.D. Bu, T.W. Noh, J. Lee, H.D. Kim, T.H. Kim, W. Jo, Differences in nature of defects between $SrBi_2Ta_2O_9$ and $Bi_4Ti_3O_{12}$, Appl. Phys. Lett. 74 (1999) 1907–1909.
[42] A.Z. Simões, E.C. Aguiar, A.H.M. Gonzalez, J. Andrés, E. Longo, J.A. Varela, Strain behavior of lanthanum modified $BiFeO_3$ thin films prepared via soft chemical method, J. Appl. Phys. 104 (2008) 104115–104120.